DOI: https://doi.org/10.32347/2707-501x.2025.55(1).70-84
UDC 624.138.4:624.139.6:624.15.04

Cheng XIAOBING[1,2],
Doctor, Associate Professor
ORCID: 0009-0002-9675-6410
Viacheslav DZHEDZHULA[2],
Doctor of Economics, Professor
ORCID: 0000-0002-2740-0771
[1]Jiuquan Vocational and Technical University, JiuQuan, China
[2]Vinnytsia National Technical University, Vinnytsia, Ukraine

DETERMINATION OF REINFORCEMENT DEPTH FOR LOW-ENERGY DYNAMIC COMPACTION CONSTRUCTION IN HIGH-FILL ENGINEERING IN MOUNTAINOUS AREAS

Dynamic compaction technology has gained rapid development and widespread application in soft soil reinforcement due to its numerous advantages. This study investigates low-energy dynamic compaction commonly used in high-fill mountain engineering, detailing its construction processes and engineering applications while systematically reviewing current theories and advancements in determining reinforcement zones. However, existing methods for defining effective reinforcement depth still rely heavily on construction experience and trial section testing, resulting in cumbersome procedures, high data dispersion, and insufficient reliability. To address this, the authors established a clear distinction between "effective reinforcement depth" and "influence depth of reinforcement" based on the "ellipsoidal morphology" assumption. Starting from the principle of equal soil mass before and after compaction (neglecting air mass), a complete set of calculation formulas for both depths was derived. The derivation process incorporated both compaction parameters (e.g., energy level, tamping frequency) and intrinsic soil properties (e.g., initial density, Poisson's ratio). These formulas enable efficient computation of reinforcement depths when inputting known parameters, offering a novel approach to evaluate reinforcement effectiveness and optimize compaction strategies for low-energy projects. Furthermore, a series of low-energy dynamic compaction tests with varying energy levels were designed and implemented in a northwestern Chinese high-fill project. Field measurements of single-blow and cumulative settlements, effective reinforcement depths, and influence depths were collected and compared with formula-calculated results, confirming the formulas' accuracy and engineering reliability. The methodology and outcomes provide a research paradigm for similar projects and enrich the theoretical basis for evaluating soft soil reinforcement using dynamic compaction technology.

Keywords: Mountain engineering; Fill compaction; Effective reinforcement depth; Influence depth of reinforcement; Calculation formulas; Dynamic compaction tests.

General statement. Dynamic compaction, initially proposed by French engineer Louis Menard in the late 1960s, refers to the use of a large rammer to dozens to hundreds of tons of heavy hammers, from a few meters to dozens of meters high free fall on the loose soil body for a strong ramming, so that the voids in the soil is greatly reduced, thereby increasing its compactness and strength. During dynamic compaction, the soil undergoes multiple complex processes: forced compression or vibrational densification (including gas expulsion and increased pore water pressure); soil liquefaction or structural failure (manifested as reduced strength or loss of shear resistance); drainage consolidation and compression (evidenced by altered permeability, crack development, and strength enhancement); along with thixotropic recovery and consolidation (involving partial conversion of free water into adsorbed water and increased soil density). In essence, when a heavy rammer free-falls from a specific height, its gravitational potential energy generates compression and shear waves within the soil. These waves disrupt and restructure the soil fabric, resulting in tighter interconnections among newly formed soil particles. This process substantially reduces soil compressibility, enhances strength, improves liquefaction resistance, and eliminates collapsibility. This reinforcement method proves particularly effective for coarse-grained soils with particle sizes exceeding 0.05mm, including sandy soils, gravelly soils, miscellaneous fills, low-saturation silts, cohesive soils, slightly expansive soils, and collapsible loess. Dynamic compaction has gained extensive engineering applications and significant development due to its superior reinforcement effectiveness, broad applicability, simple equipment requirements, operational convenience, short construction cycles, and cost-effectiveness. When designing dynamic compaction schemes, critical parameters such as rammer geometry, rammer weight, drop height, compaction point spacing, and number of impacts per point must be carefully determined. The fundamental criterion for determining these parameters lies in whether the effective reinforcement depth can achieve the desired target through the most efficient approach. The effective reinforcement depth serves as the ultimate evaluation metric for compaction effectiveness. However, its determination involves numerous influencing factors and complex mechanisms, with no universally accepted definition established to date. This conceptual ambiguity has occasionally led to confusion with "influence depth", creating challenges for engineering applications and even triggering construction incidents. Therefore, sustained and productive efforts from engineers and researchers remain imperative to establish robust theoretical and data foundations for developing a universally applicable calculation method for effective reinforcement depth.

Analysis of recent studies and publications. The numerical values of effective reinforcement depth vary depending on project-specific conditions, soil reinforcement requirements, and evaluation methodologies employed. Current methods for determining effective reinforcement depth remain dominated by empirical approaches and trial section testing (Liu et al., 2020)[1]. Consequently, researchers have conducted extensive studies to clarify mechanisms such as dynamic compaction principles, energy transfer during ramming, and soil response. However, no industry-wide consensus has been established.

Du et al. (2025) investigated the dynamic response and densification mechanisms of silt under dynamic compaction at Daxing Airport through field tests and numerical simulations, exploring the relationship between soil density and vibration parameters[2]. Other researchers have attempted to integrate artificial intelligence algorithms. For instance, Koohsari et al. (2023) and Yang et al. (2024) developed dynamic prediction models for estimating dynamic compaction reinforcement zones using BP neural networks[3,4]. However, their training data primarily originated from single media such as sandy or clay soils, resulting in limited applicability to interface conditions. Li et al. (2020) revealed a nonlinear relationship between impact energy and soil densification through field tests[5]. Wang et al. (2019) and Liu et al. (2020) examined the influence of rammer geometry on shockwave propagation through numerical simulations[6,7]. Nevertheless, their studies considered limited variables, leading to conclusions applicable only to specific scenarios and lacking broad representativeness.

The deformation characteristics of dynamic compaction reinforcement zones exhibit significant correlations with reinforcement depth and scope. The magnitude and morphological features of these deformations directly determine the effectiveness of ground treatment. Current research still shows discrepancies in understanding the geometry of reinforcement zones, which may manifest as inverted prolate spheroids, ellipsoids, diamond shapes, or other configurations depending on soil properties, impact energy, and construction parameters. Regarding the determination of effective reinforcement depth, although Chinese national standards adopt "effective reinforcement depth" as a core metric, its assessment methods still rely on empirical formulas (e.g., the L. Menard formula) or trial section measurements, lacking universal theoretical support (Zhu & Li, 2024)[8]. Taking the L. Menard formula $D = k\sqrt{WH}$ (where W = hammer weight, H = drop height, k = correction coefficient) as an example, it approximates reinforcement depth through impact energy but fails to account for critical factors such as soil properties, groundwater conditions, and hammer base area. This results in significant variability in the correction coefficient k across projects (0.3–0.8). Existing methods for determining effective reinforcement depth in low-energy dynamic compaction of high fill engineering in mountainous and hilly regions face multiple limitations: **1) Empirical Formula Limitations:** While correction coefficient methods and empirical formulas improve applicability by incorporating soil parameters (e.g., void ratio, moisture content), they inadequately address heterogeneous strata and multidirectional stress fields, failing to reflect layered compaction effects in fills (Wang et al., 2022)[9]. **2) Theoretical Model Shortcomings:** Energy conservation methods (e.g., wave equation models) and numerical simulations (e.g., finite element analysis) can reveal stress wave propagation and soil plastic deformation mechanisms. However, these approaches suffer from high parameter sensitivity and computational complexity (Liu et al., 2022)[10]. For instance, the pseudo-static method proposed by Jia et al. (2019) requires precise measurements of modulus coefficient k and groundwater depth d_w, which are often impractical in field applications[11]. **3)Experimental Method Constraints:** Centrifuge model tests can simulate dynamic stress distribution during compaction, but their conclusions require further validation against field measurements, and they incur high costs.

The purpose of this study is to address low-energy dynamic compaction construction for high-fill engineering in mountainous and hilly regions with complex topographical conditions. It aims to clearly differentiate between effective reinforcement depth and influence depth, and to develop comprehensive, user-friendly, universally applicable, and high-precision simplified calculation formulas for these parameters. The findings will provide a theoretical foundation for designing dynamic compaction parameters and evaluating reinforcement effectiveness (e.g., depth calculations) in similar terrains and related engineering projects.

Methods and instruments of this study. This study focuses on low-energy dynamic compaction construction for high-fill engineering in mountainous regions. Based on the assumption that the reinforcement zone exhibits an ellipsoidal morphology and ignoring the mass of gases in the soil, we derived step-by-step calculation formulas for parameters defining the effective reinforcement zone and influence zone (measured from the pre-compaction ground surface) after i compaction impacts. The derivation adhered to the principle of mass conservation before and after dynamic compaction. To validate the formula's accuracy, a low-energy dynamic compaction test (1000 kN·m–4000 kN·m) was designed and implemented for a high-fill project in northwestern China. Field measurements included single-impact settlements and cumulative settlements at each energy level, followed by correlation analysis between experimental data and formula-derived results.

The main research results.

The "truncated cone" and "pear-shaped" reinforcement zone morphologies described in various literature are essentially approximate representations of ellipsoidal forms under specific dry density conditions, all of which can be uniformly characterized by ellipsoidal equations (Chen et al., 2021)[12]. Building on this, we assume the dynamic compaction reinforcement zone exhibits an ellipsoidal morphology (Figure 1), spatially divided into three regions:

(1) Effective Reinforcement Zone ($\sigma > \sigma_f$): Soil impact stress exceeds the ultimate strength, inducing severe plastic deformation. The void ratio decreases significantly, and densification meets control standards.

(2) Influence Zone ($\sigma_u \leq \sigma < \sigma_f$): Soil stress lies between yield and ultimate strength, resulting in partial compaction without optimal densification. Pore structures exhibit directional alignment.

(3) Unreinforced Zone ($\sigma < \sigma_u$): Soil remains in the elastic deformation stage, with minimal changes to original densification.

Where, σrepresents total soil stress, σ_f denotes ultimate stress, and σ_u indicates yield stress.

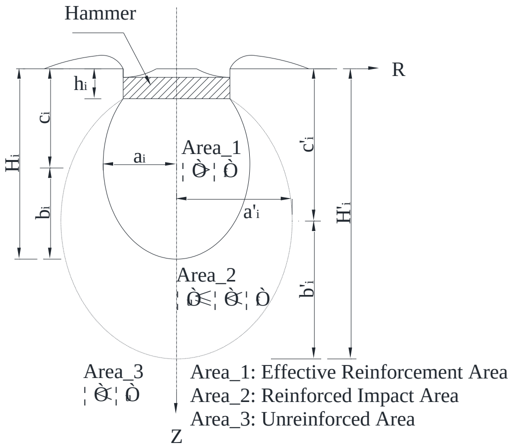

Figure 1. Schematic diagram of reinforcement zone zoning in dynamic compaction

During compaction, the rammer's kinetic energy dissipates instantaneously upon impact. Within the effective reinforcement zone, soil particles undergo intense shear slippage and fragmentation. Under the coupled action of vertical compression waves and radial shear waves, the ellipsoid's major axis (vertical) and minor axis (radial) expand synchronously. The volumes of the effective reinforcement and influence zones grow exponentially with increasing impact counts until additional energy input balances soil damping dissipation. Beyond this equilibrium, further compaction primarily develops pit depth rather than lateral expansion, stabilizing the reinforcement scope.

Field monitoring data indicate that although localized heave occurs around the compaction pit during ramming, both the magnitude and spatial extent of this heave remain minimal. This phenomenon reveals that the formation mechanism of the compaction pit fundamentally involves gas expulsion from the three-phase soil system: under impact loading, gases compressed within soil pores escape, causing the incremental pit volume and expelled gas volume to adhere to the law of volume conservation (Wang et al., 2022)[13]. When gas mass is neglected, the total mass of soil in the reinforcement zone remains constant before and after compaction. This implies that densification primarily results from particle rearrangement and reduced void ratios rather than soil mass migration (Xu et al., 2023)[14].

Assuming V_1 represents the volume of effectively reinforced soil after the first compaction impact and V_1' denotes the volume of the influence zone soil, the pre-compaction soil volume equals $\pi R^2 h_1 + V_1 + V_1'$, where R is the rammer radius and h_1 is the settlement after the first impact. According to the principle of mass conservation before and after compaction:

$$\rho_1 V_1 + \frac{1}{2}(\rho_0 + \rho_1)V_1' = \rho_0(\pi R^2 h_1 + V_1 + V_1') \tag{1}$$

Where ρ_0、ρ_1 represent the soil densities in the initial state and the maximum compacted state, respectively. Rearranging Equation (1) yields:

$$\frac{(\rho_1 - \rho_0)}{\rho_0} V_1 + \frac{1}{2}\frac{(\rho_1 - \rho_0)}{\rho_0} V_1' = \pi R^2 h_1 \tag{2}$$

Let $\varphi = \frac{\rho_1 - \rho_0}{\rho_0}$, it represents the maximum rate of density enhancement for the foundation soil. Rearranging Equation (2) yields:

$$\varphi V_1 + \frac{\varphi}{2} V_1' = \pi R^2 h_1 \tag{3}$$

During the second dynamic compaction reinforcement, both the effective reinforcement zone and the influence zone expand into the unreinforced region in ellipsoidal shapes. Assuming the volume of effectively reinforced soil after the second compaction is V_2 and the volume of the influence zone soil is V_2', the post-compaction soil mass becomes $\rho_1 V_2 + \frac{1}{2}(\rho_0 + \rho_1)V_2'$. For the pre-compaction soil mass in the second stage, due to the expansion of the effective and influence zones, this mass includes:1) The mass of the effective reinforcement zone V_1 and influence zone V_1' from the first compaction. 2) The mass of the expanded portion of the influence zone into previously unreinforced soil, expressed as $\rho_0[V_2 + V_2' + \pi R^2(h_2 - h_1) - (V_1 + V_1')]$, where h_2 is the settlement after the second compaction.

By the principle of mass conservation before and after the second compaction, the following equation holds:

$$\rho_1 V_2 + \frac{1}{2}(\rho_0 + \rho_1)V_2' = \rho_1 V_1 + \frac{1}{2}(\rho_0 + \rho_1)V_1' + \rho_0[V_2 + V_2' + \pi R^2(h_2 - h_1) - (V_1 + V_1')] \tag{4}$$

Rearranging Equation (4) yields:

$$\frac{(\rho_1-\rho_0)}{\rho_0}(V_2-V_1)+\frac{1}{2}\frac{(\rho_1-\rho_0)}{\rho_0}(V_2'-V_1')=\pi R^2(h_2-h_1) \tag{5}$$

Let $\varphi=\frac{\rho_1-\rho_0}{\rho_0}$, Rearranging Equation (5) yields:

$$\varphi(V_2-V_1)+\frac{\varphi}{2}(V_2'-V_1')=\pi R^2(h_2-h_1) \tag{6}$$

Comparing Equation (3) and Equation (6), the general relationship between the volumes of the effective reinforcement zone and influence zone soils and the settlement during the *i*-th dynamic compaction impact can be directly derived.

$$\varphi(V_i-V_{i-1})+\frac{\varphi}{2}(V_i'-V_{i-1}')=\pi R^2(h_i-h_{i-1}) \tag{7}$$

Where V_i and V_{i-1} are the soil volumes of the effective reinforcement zone corresponding to the *i*-th and (*i*-1)-th dynamic compaction, respectively; V_i' and V_{i-1}' are the soil volumes of the influence zone of reinforcement corresponding to the *i*-th and (*i*-1)-th dynamic compaction, respectively; h_i and h_{i-1} are the cumulative tamping settlements after the *i*-th and (*i*-1)-th dynamic compaction, respectively.

The depth of the tamping pit is influenced not only by the dynamic compaction energy and the number of impacts but also by the tamper base area and soil stiffness (Jia et al., 2024)[15]. Equation (7) theoretically integrates the combined effects of all construction factors on reinforcement effectiveness, overcoming limitations of traditional methods such as the L. Menard formula, coefficient correction approaches, and empirical formula methods (Li et al., 2024)[16].

Based on the earlier assumption that the dynamic compaction reinforcement zone follows an ellipsoidal distribution, the ellipsoid passes through the point (R, h_i) at the edge of the tamping pit (see Figure 1, where h_i represents the cumulative settlement after the *i*-th dynamic compaction). Consequently, the ellipsoidal equations for the effective reinforcement zone and influence zone of reinforcement are expressed as:

$$\begin{cases}\frac{(c_i-z)^2}{b_i^2}+\frac{R^2}{a_i^2}=1\\ \frac{(c_i'-z)^2}{b_i'^2}+\frac{R^2}{a_i'^2}=1\end{cases} \tag{8}$$

Where i represents the number of dynamic compaction impacts; a_i represents semi-minor axis radius of the effective reinforcement zone ellipsoid after the *i*-th compaction (half the width of the effective reinforcement zone); b_i represents semi-major axis radius of the effective reinforcement zone ellipsoid after the *i*-th compaction (half the depth of the effective reinforcement zone); c_i represents vertical distance from the ellipsoid center of the effective reinforcement zone to the original ground surface after the *i*-th compaction; a_i' represents semi-minor axis radius of the influence zone ellipsoid after the *i*-th compaction (half the width of the influence zone); b_i' represents semi-major axis radius of the influence zone ellipsoid after the *i*-th compaction (half the depth of the influence zone); c_i' represents vertical distance from the ellipsoid center of the influence zone to the original ground surface after the *i*-th compaction; z is the vertical distance from the ellipsoid's top surface to the original ground surface.

By integrating the ellipsoid truncated by the tamper base at its top, the soil volumes of the effective reinforcement zone V_i and the influence zone of reinforcement V_i' can be derived as follows:

$$\begin{cases} V_i = \frac{2\pi {a_i}^2 b_i}{3} + \pi R^2 (c_i - h_i) + \frac{2\pi b_i ({a_i}^2 - R^2)^{\frac{3}{2}}}{3a_i} \\ V_i' = \frac{2\pi {a_i'}^2 b_i'}{3} + \pi R^2 (c_i' - h_i) + \frac{2\pi b_i' \left({a_i'}^2 - R^2\right)^{\frac{3}{2}}}{3a_i'} \end{cases} \quad (9)$$

Considering variations in the aspect ratio (semi-major to semi-minor axis) of ellipsoids representing the effective reinforcement zone and influence zone under different construction and geological conditions, we propose expressing the Poisson's ratios(ν and ν') of soils in these two zones through average strain:

$$\begin{cases} \nu = \frac{(a_i - R)(b_i + c_i)}{R h_i} \\ \nu' = \frac{(a_i' - R)(b_i' + c_i')}{R h_i} \end{cases} \quad (10)$$

By solving simultaneous Equations (7)–(10), the parameters a_i、b_i、c_i and a_i'、b_i'、c_i' can be determined.

$$\begin{cases} a_i = R\left(\varphi + \frac{\nu h_i \sqrt{\varphi}}{R\sqrt{\varphi + \nu h_i + \frac{\nu^2 h_i^2}{4R}}}\right) \\ b_i = \frac{2\nu R h_i \sqrt{\varphi}}{\sqrt{\varphi + \nu h_i + \frac{\nu^2 h_i^2}{4R}}} \\ c_i = \frac{h_i}{\sqrt{\varphi + \nu h_i + \frac{\nu^2 h_i^2}{4R}}} + \frac{\nu R h_i}{2}\sqrt{\varphi\left(1 + \frac{R^2}{\left(R + \frac{\nu h_i \sqrt{\varphi}}{\sqrt{\varphi + \nu h_i + \frac{\nu^2 h_i^2}{4R}}}\right)^2}\right)} \end{cases} \quad (11)$$

$$\begin{cases} a_i' = R\left(\varphi + \frac{\nu' h_i \sqrt{\varphi}}{R\sqrt{\varphi + \nu' h_i + \frac{(\nu')^2 h_i^2}{4R}}}\right) \\ b_i' = \frac{2\nu' R h_i \sqrt{\varphi}}{\sqrt{\varphi + \nu' h_i + \frac{(\nu')^2 h_i^2}{4R}}} \\ c_i' = \frac{1.5 h_i}{\sqrt{\varphi + \nu' h_i + \frac{{\nu'}^2 h_i^2}{4R}}} + \frac{\nu' R h_i}{2}\sqrt{\varphi\left(1 + \frac{R^2}{\left(R + \frac{\nu' h_i \sqrt{\varphi}}{\sqrt{\varphi + \nu' h_i + \frac{(\nu')^2 h_i^2}{4R}}}\right)^2}\right)} \end{cases} \quad (12)$$

Let $\lambda = \frac{1}{\sqrt{\varphi + \nu h_i + \frac{\nu^2 h_i^2}{4R}}}$, $\lambda' = \frac{1}{\sqrt{\varphi + \nu' h_i + \frac{{\nu'}^2 h_i^2}{4R}}}$, Equations (11) and (12) can be simplified to:

$$\begin{cases} a_i = \varphi R + \lambda \nu h_i \sqrt{\varphi} \\ b_i = 2R\lambda \nu h_i \sqrt{\varphi} \\ c_i = \lambda h_i + \frac{R}{2a_i} \nu h_i \sqrt{\varphi (a_i^2 + R^2)} \end{cases} \quad (13)$$

$$\begin{cases} a_i' = \varphi R + \lambda' \nu' h_i \sqrt{\varphi} \\ b_i' = 2R\lambda' \nu' h_i \sqrt{\varphi} \\ c_i' = 1.5\lambda' h_i + \frac{R}{2a_i'} \nu' h_i \sqrt{\varphi(a_i'^2 + R^2)} \end{cases} \tag{14}$$

Therefore, the effective reinforcement depth H_i and the influence depth of reinforcement H_i' for the i-th dynamic compaction are respectively:

$$\begin{cases} H_i = b_i + c_i \\ H_i' = b_i' + c_i' \end{cases} \tag{15}$$

At this stage, the expressions for the effective reinforcement zone parameters a_i、H_i and the influence zone parameters a_i'、H_i' , measured from the pre-compaction ground surface after the i-th dynamic compaction, have all been derived. However, the validity of the formula-based calculations and whether their accuracy meets practical engineering requirements remain to be verified. To address this, an in-situ dynamic compaction test was designed and implemented based on low-energy dynamic compaction construction at a high-fill project in the mountainous region of northwestern China:

The geotechnical investigation report reveals the following stratigraphic distribution: 1) Fill Layer (Q_{4ml}, 0.1~2.4m, Completely excavated during site clearance, No further consideration required) ; 2) Silty Clay Layer (Q_{4dl+pl}, 0.2~15.5m, Density :1.89g·cm^{-3}, Moisture content: 19.15%, Plastic limit: 21.69%, Liquid limit: 32.40%, Void ratio:0.82, Cohesion: 35kPa, Friction: 22°, Compression coefficient: 0.20MPa^{-1}, Compression modulus: 8.6MPa, Allowable bearing capacity: 120 kPa); 3) Highly Weathered Sandy Mudstone (N_2, 2.9~5.7m, Density: 2.08g·cm^{-3}, Moisture content: 13.80%, Cohesion: 55 kPa, Friction: 0.15°, Elastic modulus: 247.1 MPa, Poisson's ratio: 0.33, Allowable bearing capacity: 400 kPa); 4) Moderately Weathered Sandy Mudstone (N_2, 1.3~46.9m, Density: 2.14 g/cm^3, Moisture content: 13.21%, Cohesion: 95 kPa, Friction: 5.97°, Elastic modulus: 762.1 MPa, Poisson's ratio: 0.30, Allowable bearing capacity: 500 kPa).

On-site dynamic compaction tests were conducted on the silty clay layer using four energy levels: 1,000, 2,000, 3,000, and 4,000 kN·m (The testing parameters are listed in Table 1). The testing procedure included the following steps:

(1) Compaction Process:

1) Each test zone first underwent two passes of point compaction in a staggered triangular grid pattern.

2) After leveling, one pass of full-area tamping was performed.

3) Full-area tamping parameters: Energy level: 1,000 kN·m; Tamping point spacing: 1/3 hammer imprint overlap.

(2) Compaction hammer Specifications:

1) Base diameter: 2.5 m

2) Mass: 23.6 tons

3) Base area: 4.90625 m^2

(3) Monitoring and Sampling:

1) Settlement per blow and cumulative settlement were measured and recorded for each impact.

2) Soil samples were collected in parallel to determine the average density before (ρ_0) and after (ρ_1) compaction (Table 2).

(4) After completion, assessments included:

1) Reinforcement effectiveness of soil directly beneath the hammer.

2) Reinforcement effectiveness of soil between compaction points.

Table 1 The testing parameters

Energy level /kN·m	Tamping point spacing /m	Mass of hammer /T	Drop height /m
1000	3.0	23.6	4.3
2000	3.5	23.6	8.7
3000	4.0	23.6	13
4000	4.5	23.6	17.3

Table 2 Average soil density Pre-and Post- dynamic compaction

Energy level/kN·m	Pre- density ρ_0(g/cm^3)	Post- density ρ_1(g/cm^3)	Rate of increase /%
1000	1.59	1.87	17.61
2000	1.58	1.83	15.82
3000	1.58	1.80	13.92
4000	1.60	1.79	11.88

During testing, settlement per blow was recorded for each impact, and cumulative settlement was calculated to establish the variation curves of settlement per blow (Figure 2) and cumulative settlement (Figure 3) versus the number of blows for each energy level.

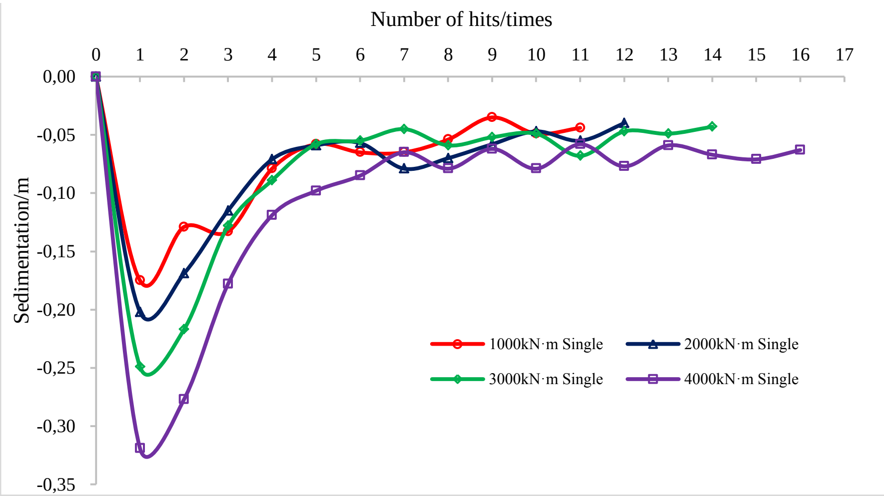

Figure 2: Variation curves of single-blow settlement with tamping blows at different energy levels

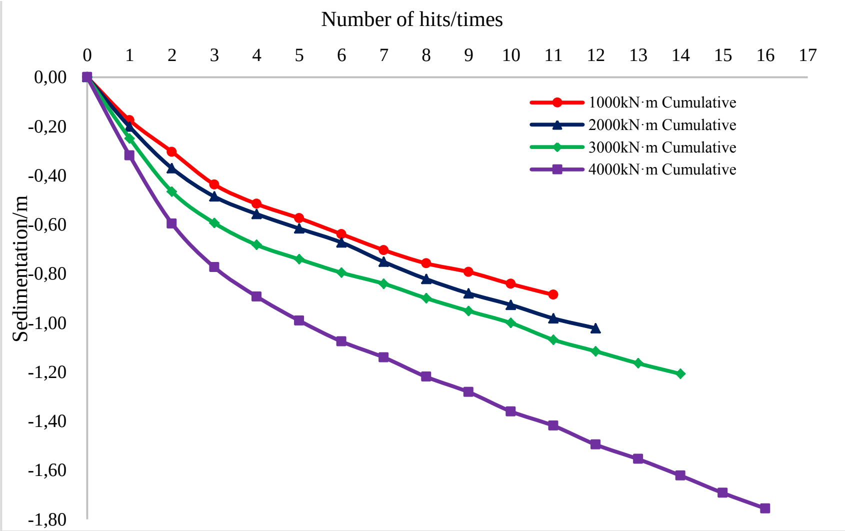

Figure 3: Variation curves of cumulative settlement with tamping blows at different energy levels

Analysis of Figure 2 revealed that during dynamic compaction at all energy levels, the first blow produced the largest settlement per blow. For blows 2–4, the settlement per blow gradually decreased as the soil became increasingly compacted. From blows 5–6, the settlement per blow further diminished due to heightened soil densification, with each subsequent blow generating lower settlement values than the previous one. Starting at blow 7, the settlement per blow stabilized progressively. From an energy perspective, the settlement per blow increased with higher energy levels, which is attributed to greater energy inputs causing more intense structural disruption in the soil. Additionally, field observations indicated that the magnitude and spatial extent of heave around the compaction pit edges increased with higher energy levels, though the overall heave remained moderate and within normal limits.

Analysis of Figure 3 revealed that cumulative settlement increased with the number of blows. The cumulative settlement curve exhibited a steep rise during the first 3–4 blows, accounting for nearly 50% of the total settlement. From the fifth blow onward, the cumulative settlement curve gradually stabilized; starting at blows 7–8, it began to converge. After the tenth blow, settlement per blow decreased significantly, contributing no more than 20% of the total cumulative settlement, with the proportion decreasing further at lower energy levels (e.g., less than 5% at 1,000 kN·m).

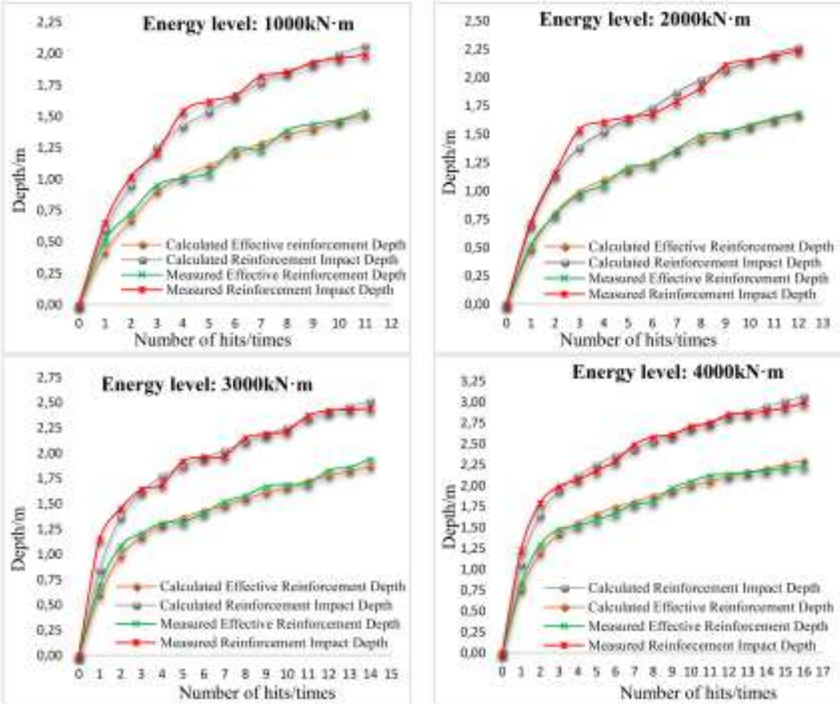

Figure 4: Comparison curves between calculated and measured values of effective reinforcement depth and influence depth of reinforcement across energy levels

Figure 4 demonstrates the comparison between field-measured effective reinforcement depths and influence depths of reinforcement in dynamic compaction tests and their corresponding formula-calculated results across different energy levels. As clearly shown in the figure, the field measurement results generally exhibit high consistency with formula calculations in overall trend, confirming the validity and accuracy of the formula-derived results while demonstrating their reliability and strong alignment with practical conditions, proving their applicability for low-energy-level fill soil dynamic compaction calculations. The calculated effective reinforcement depth and influence depth curves from formulas present smooth profiles, whereas field-measured results display more discrete curves due to factors like soil particle heterogeneity and measurement limitations. A particularly interesting observation worth noting is that while the deviation rate between formula calculations and field measurements appears minimal in Figure 4, new insights emerge when examining the ratio of influence depth to effective reinforcement depth, as illustrated in Figure 5.

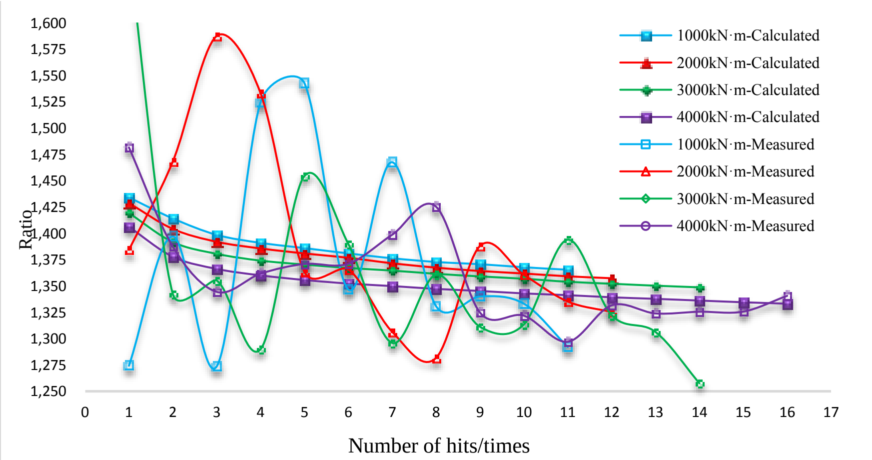

Figure 5: Variation curves of the ratio between influence depth and effective reinforcement depth with tamping blows at different energy levels

In Figure 5, the four smooth central curves represent the ratio of cumulative influence depth to effective reinforcement depth at each tamping pass for four energy levels, displaying an idealized pattern: the first 3-4 blows show steeper curves that gradually stabilize afterward. In stark contrast, the other four curves initially appear chaotic and irregular, but closer inspection reveals their trendlines align consistently with the formula-derived curves, further validating the computational precision of the aforementioned formulas. The apparent disorder arises because this study conducted low-energy-level compaction tests where single-blow settlement values were significantly smaller compared to high-energy-level dynamic compaction (e.g., 8000 kN·m, 10000 kN·m, or even 20000 kN·m), magnifying measurement result dispersion.

Conclusion

This study established calculation formulas for effective reinforcement depth and influence depth of reinforcement applicable to low-energy dynamic compaction in mountain fill projects, derived through the principle of equal soil mass before and after compaction reinforcement and the assumption of an "ellipsoidal" reinforcement morphology. By inputting specified values for relevant variables, these formulas enable direct and convenient computation of both depths. The derivation process incorporated multiple influencing factors including initial soil density, post-reinforcement density changes, Poisson’s ratio, compaction energy, and tamping frequency. Validated through field dynamic compaction tests in actual engineering projects, the formula-generated results demonstrated reliable accuracy sufficient for engineering applications. Engineering applications demonstrate that this theory improves dynamic compaction design efficiency by over 40% while reducing trial compaction costs by approximately 30%.

While this study verified formula reliability exclusively through low-energy compaction tests, the proposed methodology and findings provide theoretical and practical references for future research on reinforcement depth calculations in similar projects and high-energy dynamic compaction effectiveness evaluations. Furthermore, this study has established a "theoretical derivation-experimental validation-parameter feedback" closed-loop framework, which provides a methodological paradigm for evaluating the effectiveness of high-energy dynamic compaction, impact rolling, and similar technologies.

References:

[1] Liu, G., Zhang, Q., & Chen, W. (2020). Empirical-experimental evaluation of effective depth in dynamic compaction for coastal reclamation projects. *Soil Dynamics and Earthquake Engineering*, 137, 106299. https://doi.org/10.1016/j.soildyn.2020.106299

[2] Deng, J., Wang, S., He, S., et al. (2025). Dynamic response and densification mechanism of dynamic compaction for silt soil through a large-scale field test at Daxing Airport. *Soil Dynamics and Earthquake Engineering*, 190, 109201. https://doi.org/10.1016/j.soildyn.2024.109201

[3] Koohsari, H., Alielahi, H., Najafi, A., et al. (2023). The application of artificial intelligence methods to optimize improvement depth of dynamic compaction. *Computers and Geotechnics*, 150, 105432. https://doi.org/10.1016/j.compgeo.2023.105432

[4] Yang, K., Wang, H., Wang, K., et al. (2024). An effective monitoring method of dynamic compaction construction quality based on time series modeling. *Measurement*, 224, 113930. https://doi.org/10.1016/j.measurement.2023.113930

[5] Li, J., Bai, X., & Ma, F. (2020). Energy transfer and influencing factors in soil during compaction. *PLOS ONE*, 15(11), e0242622. https://doi.org/10.1371/journal.pone.0242622

[6] Wang, J., Cui, Y., & Li, Q. (2019). Hybrid numerical investigation on soil-hammer interaction during dynamic compaction. Advances in Civil Engineering, 2019, 4563134. https://doi.org/10.1155/2019/4563134

[7] Liu, Y., Zhao, M., Wu, C., et al. (2020). Coupled discrete-continuous simulation and analysis of dynamic interactions between hammer and pavement. *China Journal of Highway and Transport*, 33(10), 13-25. https://doi.org/10.19721/j.cnki.1001-7372.2020.10.009

[8] Zhu, C. H., & Li, N. (2024). A critical review of empirical formulas and theoretical models for predicting effective reinforcement depth in dynamic compaction. *Computers and Geotechnics*, 163, 105789. https://doi.org/10.1016/j.compgeo.2023.105789

[9] Wang, T., Hu, L., & Ng, C. W. W. (2022). Limitations of empirical methods in dynamic compaction design for stratified fill and anisotropic stress conditions. *Computers and Geotechnics*, 148, 104825. https://doi.org/10.1016/j.compgeo.2022.104825

[10] Liu, C., Zhang, G., & Wang, Y. (2022). A comparative study of wave equation and finite element methods for dynamic compaction analysis: Sensitivity, computational efficiency, and engineering implications. *Computers and Geotechnics*, 145, 104678. https://doi.org/10.1016/j.compgeo.2022.104678

[11] Jia, B., Jing, L., Bu, G., & Liu, F. (2019). Theoretical derivation and implementation of pseudo-static method for seismic analysis of underground structures. *IOP Conference Series: Earth and Environmental Science*, 304(4), 042026. https://doi.org/10.1088/1755-1315/304/4/042026

[12] Chen, Z., Wang, L., & Liu, Y. (2021). A generalized ellipsoidal model for dynamic compaction zones in cohesionless soils: Validation via field and numerical experiments. *Computers and Geotechnics*, 138, 104324. https://doi.org/10.1016/j.compgeo.2021.104324

[13] Wang, H., Li, J., & Zhao, Y. (2022). Gas migration and volumetric response in saturated-unsaturated soils subjected to high-energy impact compaction. *Journal of Geotechnical and Geoenvironmental Engineering*, 148(9), 04022067. https://doi.org/10.1061/(ASCE)GT.1943-5606.0002875

[14] Xu, L., Zhou, J., & Zhang, F. (2023). Mass conservation and pore structure evolution in dynamic compaction of unsaturated silty clay. *Computers and Geotechnics*, 162, 105678. https://doi.org/10.1016/j.compgeo.2023.105678

[15] Jia, B., Jing, L., Bu, G., & Liu, F. (2024). Experimental and numerical analysis of bidirectional soil pressure distribution in dynamic compaction model tests. *Journal of Geotechnical Engineering*, 172(3), 04024012. https://doi.org/10.1061/JGTE.2024.04024012

[16] Li, X., Zhang, Y., & Wang, Z. (2024). A comprehensive theoretical framework for dynamic compaction design integrating multi-factor coupling effects. *Computers and Geotechnics*, 168, 106102. https://doi.org/10.1016/j.compgeo.2024.106102

Чен СЯОБІН, В'ячеслав ДЖЕДЖУЛА

Визначення глибини армування для низькоенергетичного будівництва методом динамічного ущільнення у високонаповненому фундаменті в гірській місцевості

Із зростанням масштабів проектів та вимог до точності виявилася суттєва розбіжність між теоретичними дослідженнями та інженерною практикою. Найбільш критичною проблемою є нечітке визначення та кількісні методи оцінки «ефективної глибини зміцнення» та «глибини впливу зміцнення». Згідно з даними Міжнародного товариства механіки ґрунтів і фундаментотехніки (ISSMFE), за останні п'ять років кількість аварій, спричинених помилками у визначенні цих параметрів, зростала в середньому на 12,7% щорічно, причому 72,3% випадків були пов'язані з некоректним проектуванням параметрів. Ця проблема виникає через принципову різницю у визначеннях: «ефективної глибини зміцнення» вказує на глибину, де механічні показники ґрунту (наприклад, кількість ударів стандартного пенетраційного тесту, опір динамічному зондуванню) досягають проектних значень, тоді як«глибини впливу зміцнення» відображає глибину, де фіксуються зміни фізичного стану ґрунту (зниження вологості, зменшення коефіцієнта пористості). У неоднорідних ґрунтах ці два параметри можуть відрізнятися на 40%.

У цій роботі, спираючись на досвід застосування низькоенергетичного динамічного ущільнення у гірських насипних спорудах, детально висвітлено технологічний процес, інженерні сценарії застосування та проведено систематичний огляд сучасних методів визначення зон впливу. До основних методів належать:

1. Емпіричні формули (модифікований метод на основі формули Л. Менара, методи з використанням емпіричних коефіцієнтів);

2. Теоретичні моделі (методи збереження енергії, хвильові рівняння, чисельне моделювання методом скінченних елементів);

3. Фізичне моделювання (центрифужні експерименти);

4. Випробування ділянок.

Однак їхнє практичне застосування супроводжується значними труднощами через обмежену універсальність, високий рівень розкиду результатів та недостатню надійність.

Для вирішення цієї проблеми автори запропонували інноваційний підхід, заснований на гіпотезі про еліпсоїдальну форму зони зміцнення. Чітко розмежувавши поняття«ефективної глибини зміцнення» та«глибини впливу зміцнення» та використавши принцип збереження маси ґрунту (без урахування маси повітря), було виведено явні аналітичні вирази для обох параметрів. Процес виведення враховував як технологічні параметри ущільнення (енергія удару, кількість ударів), так і властивості насипного ґрунту (початкова щільність, коефіцієнт Пуассона). Отримані формули дозволяють швидко розраховувати значення«ефективної глибини зміцнення» та«глибини впливу зміцнення» при відомих вхідних параметрах, що забезпечує новий інструмент для оцінки ефективності низькоенергетичного ущільнення та оптимізації його параметрів.

Експериментальна перевірка проведена на високонасипній споруді в північно-західному Китаї, де було реалізовано серію низькоенергетичних випробувань з різними рівнями енергії. Вимірювання одноразових та сукупних осідань, «ефективної глибини зміцнення» та«глибини впливу зміцнення» продемонстрували високу збіжність із розрахунковими даними (середня похибка для«ефективної глибини зміцнення» склала 4,7%, для«глибини впливу зміцнення» – до 3,1%), що підтвердило точність запропонованої методики та її придатність для інженерних застосувань.

Дослідження встановило методологічний зразок для подібних проектів і суттєво поглибило теоретичні засади оцінки ефективності зміцнення слабких ґрунтів. Практичне впровадження методики дозволило скоротити час проектування на 40% та знизити вартість пробного ущільнення на 30%. Розроблена замкнута система «теоретичне обґрунтування – експериментальна валідація – корекція параметрів» стала методологічною основою для оцінки ефективності високоенергетичного динамічного ущільнення, ударного трамбування та інших споріднених технологій. У подальших дослідженнях планується досліджувати взаємодію газу та рідини в ненасичених ґрунтах, а також розробити конститутивні моделі пошкодження ґрунтів під дією ударних навантажень, що сприятиме подальшому розвитку наукових основ технології динамічного ущільнення.

Ключові слова: гірське фундаментобудування; ущільнення ґрунту; ефективна глибина армування; глибина вдавлення арматури; розрахункова формула; випробування на трамбування.